

Optimal Control to Minimize Dissipation and Fluctuations in Open Quantum Systems Beyond Slow and Rapid Regimes

Yuki Kurokawa and Yoshihiko Hasegawa

*Graduate School of Information Science and Technology,
The University of Tokyo, Bunkyo-ku, 113-8656 Tokyo, Japan*

Optimal control is a central problem in quantum thermodynamics. While control theories in the rapid-driving and slow-driving limits have been developed, to the best of our knowledge there is no general optimization method applicable to intermediate timescales. We introduce an optimal-control framework to minimize dissipated work and work variance, defined via the two-point measurement scheme, in open quantum systems governed by time-dependent Lindblad master equations. By introducing an auxiliary operator, we convert the history-dependent work variance into a time-local integral, enabling efficient gradient-based optimization beyond slow or rapid driving regimes. Applying our method, we find that in the coherent spin–boson model the optimized protocol can switch discontinuously between distinct locally optimal solutions as the relative weight between dissipation and fluctuations is varied. Moreover, for a single-level quantum dot coupled to a fermionic reservoir, the optimized fluctuation-minimizing protocol develops a qualitatively different multi-step structure that is not captured by approaches based on slow- or rapid-driving limits.

I. INTRODUCTION

The optimization of driving protocols that minimize dissipation and fluctuations is a central theme in nonequilibrium stochastic thermodynamics [1]. For classical systems such as a Brownian particle, protocols that minimize the mean dissipated work for a fixed total duration are known to exhibit jumps at the beginning and at the end of the protocol [2, 3]. Jump protocols have also been found in minimizing dissipation and work fluctuations in rapidly driven classical systems [4]. In the slow-driving regime, linear-response theory leads to a work fluctuation–dissipation relation in which the dissipated work is proportional to the work variance [5]. At intermediate driving speeds, numerical optimization of smooth protocols reveals richer behavior, including phase-transition-like changes in the optimal protocol structure when trading off mean dissipation against work fluctuations [6].

Defining work in quantum mechanics is nontrivial because, unlike classical work, it is not represented by a single Hermitian observable in general [7]. In particular, the naive operator identification $W = H(\tau) - H(0)$ does not, in general, reproduce the correct work statistics and is incompatible with quantum fluctuation relations beyond special cases [25]. A standard and widely used resolution is the two-point measurement (TPM) scheme [8–12]. In the TPM scheme, one performs projective energy measurements at the beginning and end of the protocol and defines the stochastic work as the difference of the two outcomes, $w = E_f - E_i$. If the initial state carries quantum coherence in the energy eigenbasis, the first projective measurement removes it and thus modifies the subsequent dynamics; this is an intrinsic limitation of the TPM definition. Nevertheless, TPM work satisfies the quantum Jarzynski equality and related fluctuation theorems [10–14], and it is the prevailing framework for characterizing work statistics in driven open quantum

systems [15–17].

In limiting regimes, for open quantum systems governed by Lindblad dynamics [18, 19], optimal protocols that minimize dissipated work and work fluctuations within the TPM framework have been obtained analytically. In the slow-driving limit, where the dynamics remains close to quasistatic, quantum generalizations of the classical fluctuation–dissipation relation show that quantum coherence generically prevents the simultaneous minimization of dissipated work and work variance [16, 20]. In the opposite, rapid-driving limit, protocols that minimize convex combinations of dissipated work and work variance were characterized analytically within a restricted class of protocols consisting of two jumps separated by a constant plateau [17], rather than through a general numerical optimal-control scheme.

At intermediate time scales, Pontryagin-type optimal-control techniques [22] have been applied to design finite-time driving protocols that minimize dissipation or maximize performance in Lindblad dynamics [21]. In these approaches the thermodynamic cost functionals are time-local, depending on the instantaneous state and control (for example the mean heat or entropy production), and fluctuations of TPM work are not incorporated explicitly. In particular, to the best of our knowledge, there is currently no numerical framework that treats dissipated work and TPM work fluctuations on an equal footing for general time-dependent open quantum systems.

In this work we establish such a framework by developing an optimal-control method that minimizes both dissipation and fluctuations defined within the TPM scheme for open systems governed by Lindblad dynamics beyond slow and rapid driving regimes. We consider a control parameter $u(t)$ entering both the system Hamiltonian and the dissipative rates, and introduce an auxiliary operator $Y(t)$ obeying a linear equation of motion. This auxiliary state recasts the inherently history-dependent TPM work variance, which is naturally expressed as a double time integral over two-time correlation functions, into a time-

local single integral over the enlarged state $(\rho(t), Y(t))$. In this way, a linear combination of dissipation and fluctuations can be written as a standard time-local cost functional, making it amenable to gradient-based Pontryagin/GRAPE optimal-control algorithms.

In particular, we consider

$$J = (1 - \alpha) W_{\text{diss}} + \frac{\alpha\beta}{2} \sigma_w^2 + \frac{\kappa}{2} (u_T - u(T))^2, \quad (1)$$

where W_{diss} is the dissipated work defined in the TPM scheme, σ_w^2 is the TPM work variance obtained through $Y(t)$, and the last term enforces the terminal constraint on the control parameter $u(t)$. Because both $\rho(t)$ and $Y(t)$ satisfy linear equations, the gradient of J with respect to the time-dependent control can be computed efficiently. This allows us to employ GRAPE-type gradient-based optimal control algorithms [23] based on Pontryagin's maximum principle [22] in order to obtain numerically optimal continuous protocols. We demonstrate the resulting framework on two numerical examples. First, for a driven spin-boson model controlled by a time-dependent bias field, we benchmark the optimized continuous protocols against the rapid-drive approximation: in the incoherent case ($\Delta = 0$) they reproduce the endpoint-jump and near-plateau structure at short protocol durations, while for longer durations the intermediate segment is no longer approximately constant, indicating a departure from the rapid-drive description [17]. For the coherent case ($\Delta \neq 0$), the optimized protocols depend strongly on the trade-off parameter α , and the observed missing segment in the Pareto front is consistent with a switch between distinct locally optimal protocol families. Second, for a quantum-dot model coupled to a wide-band metallic lead, the optimization yields multi-step jump protocols with an additional intermediate jump that is not captured by the rapid-drive approximation.

II. METHODS

A. Fluctuation and dissipation in the TPM scheme

We adopt the TPM scheme to define work. Let T be the protocol duration. In this setting, the mean work is given by the time-integrated power,

$$\langle W \rangle = \int_0^T \text{Tr}(\dot{H}(t) \rho(t)) dt. \quad (2)$$

We consider an open quantum system whose dynamics is described by the Lindblad equation [18]

$$\begin{aligned} \dot{\rho}(t) &= \mathcal{L}_t(\rho(t)) \\ &:= -i[H(t), \rho(t)] \\ &+ \sum_{\alpha} \gamma_{\alpha}(t) (L_{\alpha}(t) \rho(t) L_{\alpha}^{\dagger}(t) - \frac{1}{2} \{L_{\alpha}^{\dagger}(t) L_{\alpha}(t), \rho(t)\}) \end{aligned} \quad (3)$$

with jump operators $L_{\alpha}(t)$ and rates $\gamma_{\alpha}(t) \geq 0$. Throughout this work, we set $\hbar = 1$ and assume that the system is initially in the Gibbs state corresponding to $H_0 := H(0)$ at inverse temperature β ,

$$\rho(0) = \pi_0 := \frac{e^{-\beta H_0}}{Z(H_0)}, \quad Z(H) = \text{Tr}(e^{-\beta H}), \quad (4)$$

where $Z(H)$ is the partition function. The dissipated work is then defined as

$$W_{\text{diss}} := \langle W \rangle - \Delta F, \quad (5)$$

where $F(H) = -\beta^{-1} \log Z(H)$ and $\Delta F = F(H_T) - F(H_0)$.

With these conventions, the work fluctuations can be written as [15–17]

$$\sigma_w^2 = 2 \int_0^T dt_1 \int_0^{t_1} dt_2 \text{Tr} \left\{ \dot{H}(t_1) \overleftarrow{\mathcal{P}}(t_1, t_2) [S_{\rho(t_2)}(\dot{H}(t_2))] \right\}, \quad (6)$$

where

$$\overleftarrow{\mathcal{P}}(t_1, t_2) := \overleftarrow{\mathcal{T}} \exp \left(\int_{t_2}^{t_1} d\nu \mathcal{L}_{\nu} \right), \quad (7)$$

$$S_{\rho}(O) := \frac{1}{2} \{ \rho, \Delta_{\rho} O \}_{+}, \quad \Delta_{\rho} O := O - \text{Tr}(O\rho), \quad (8)$$

and $\{\cdot, \cdot\}_{+}$ denotes the anticommutator. Here $\overleftarrow{\mathcal{T}}$ is the time-ordering operator and $\overleftarrow{\mathcal{P}}(t_1, t_2)$ is the time-ordered propagator generated by \mathcal{L}_t , such that $\rho(t_1) = \overleftarrow{\mathcal{P}}(t_1, t_2) \rho(t_2)$ for $t_1 \geq t_2$.

B. Minimization of fluctuation and dissipation

We consider a quantum system whose Hamiltonian $H(u(t))$ depends on a control parameter $u(t)$, where our objective is to minimize the cost functional defined in Eq. (1). However, the work variance in Eq. (6) is nonlocal in time: the integrand at time t_1 depends on the state at earlier times $t_2 < t_1$ through the two-time propagator $\overleftarrow{\mathcal{P}}(t_1, t_2)$. Therefore, σ_w^2 cannot be directly incorporated as a running cost in the standard GRAPE formulation, where the objective functional is assumed to be of the time-local form (B2) as in Appendix B. To cast the variance minimization into this framework, we introduce an auxiliary operator $Y(t)$ defined by Eq. (9):

$$Y(t) := \int_0^t \overleftarrow{\mathcal{P}}(t, \tau) [S_{\rho(\tau)}(\dot{H}(\tau))] d\tau. \quad (9)$$

As shown in Appendix D, $Y(t)$ obeys the following time-local equation of motion:

$$\dot{Y}(t) = \mathcal{L}_t[Y(t)] + S_{\rho(t)}(\dot{H}(t)), \quad Y(0) = 0. \quad (10)$$

Substituting (9) into (6) yields the equivalent single-integral representation

$$\sigma_w^2 = 2 \int_0^T \text{Tr}(\dot{H}(t) Y(t)) dt. \quad (11)$$

Consequently, by augmenting the state with $Y(t)$, the variance contribution becomes a running cost depending only on instantaneous variables, which makes the GRAPE optimization applicable. Additionally, by treating $Y(t)$ as a state variable and storing it at each time step as we do for $\rho(t)$, $Y(t + \Delta t)$ can be updated from $Y(t)$ using Eq. (10). With this approach, we avoid the direct evaluation of the double time integral in Eq. (6) and can compute it efficiently.

Using Eqs. (2), (5), and (11), the cost functional defined in Eq. (1) can be cast into the standard form

$$J = \int_0^T L(t) dt + \phi(T), \quad (12)$$

where the running cost $L(t)$ and the terminal cost $\phi(T)$ are given by

$$L(t) = (1 - \alpha) \text{Tr}(\dot{H}(t) \rho(t)) + \alpha \beta \text{Tr}(\dot{H}(t) Y(t)), \quad (13)$$

$$\phi(T) = -(1 - \alpha) \Delta F + \frac{\kappa}{2} (u(T) - u_T)^2. \quad (14)$$

Here we used $W_{\text{diss}} = \langle W \rangle - \Delta F$ and $\langle W \rangle = \int_0^T \text{Tr}(\dot{H}(t) \rho(t)) dt$, so that the contribution $-(1 - \alpha) \Delta F$ appears in the terminal cost. The GRAPE algorithm requires the cost functional to be expressed explicitly as a functional of the control parameter. If we choose $u(t)$ as the control, the running cost depends on $\dot{u}(t)$ through $\dot{H}(t)$, and the objective is not in the standard form with respect to $u(t)$. We therefore reparameterize the control by introducing $v(t) := \dot{u}(t)$, and treat $u(t)$ as an additional state variable governed by the kinematic equation $\dot{u}(t) = v(t)$. We further assume that the Hamiltonian depends on u only through a smooth operator-valued function $G(u)$ such that

$$\dot{H}(t) = \frac{\partial H}{\partial u}(u(t)) \dot{u}(t) = G(u(t)) v(t). \quad (15)$$

Then $S_{\rho(t)}(\dot{H}(t))$ is linear in $v(t)$ and can be written as

$$S_{\rho(t)}(\dot{H}(t)) = v(t) S_{\rho(t)}(G(u(t))).$$

Upon an arbitrary vectorization [19], we denote by $\mathbf{x}(t)$ and $\mathbf{y}(t)$ the vectorized forms of $\rho(t)$ and $Y(t)$, respectively, and by $A(t)$ the matrix representation of the Lindblad generator \mathcal{L}_t , such that $\partial_t \mathbf{x}(t) = A(t) \mathbf{x}(t)$. We also introduce the vector $\mathbf{s}(\mathbf{x}(t), u(t))$ corresponding to $S_{\rho(t)}(G(u(t)))$.

With the introduction of the auxiliary operator $Y(t)$, together with the vectorization and the reparametrization of the control in terms of $v(t) = \dot{u}(t)$, the following GRAPE algorithm becomes applicable.

1. For a given trial control $v(t)$, propagate the state variables $u(t)$, $\mathbf{y}(t)$, and $\mathbf{x}(t)$ forward in time using Eqs. (16)–(18).
2. Set the terminal values of the adjoint variables according to Eqs. (19)–(21) at $t = T$.

3. Propagate the adjoint variables backward in time using the adjoint equations and the Pontryagin Hamiltonian $H_{\text{pmp}}(t)$ in Eqs. (22) and (23)–(25).

4. Compute $\delta v(t) = \partial H_{\text{pmp}} / \partial v(t)$ and update the control according to $v(t) \rightarrow v(t) - \eta \delta v(t)$, with a suitable step size $\eta > 0$.

5. Repeat steps 1–4 until convergence of the cost J .

In step 1, the dynamics of the state variables is then expressed as

$$\dot{u}(t) = v(t), \quad (16)$$

$$\dot{\mathbf{y}}(t) = A(u(t)) \mathbf{y}(t) + v(t) \mathbf{s}(\mathbf{x}(t), u(t)), \quad (17)$$

$$\dot{\mathbf{x}}(t) = A(u(t)) \mathbf{x}(t). \quad (18)$$

Next, in step 2, we associate adjoint variables $p(t)$, $\Lambda(t)$, and $\Pi(t)$ with $u(t)$, $\mathbf{y}(t)$, and $\mathbf{x}(t)$, respectively. The terminal values of the adjoint variables are determined from the terminal cost,

$$\Pi(T) = \frac{\partial \phi(T)}{\partial \mathbf{x}(T)} = \mathbf{0}, \quad (19)$$

$$\Lambda(T) = \frac{\partial \phi(T)}{\partial \mathbf{y}(T)} = \mathbf{0}, \quad (20)$$

$$\begin{aligned} p(T) &= \frac{\partial \phi(T)}{\partial u(T)} \\ &= -(1 - \alpha) \frac{\partial \Delta F}{\partial u(T)} + \kappa (u(T) - u_T). \end{aligned} \quad (21)$$

Then in step 3, the Pontryagin Hamiltonian is defined as

$$\begin{aligned} H_{\text{pmp}}(t) &= L(t) + p(t) v(t) + \Lambda(t)^\top [A(u(t)) \mathbf{y}(t) + v(t) \mathbf{s}(\mathbf{x}(t), u(t))] \\ &\quad + \Pi(t)^\top A(u(t)) \mathbf{x}(t). \end{aligned} \quad (22)$$

Their time evolution is obtained from

$$\begin{aligned} \dot{\Pi}(t) &= -\frac{\partial H_{\text{pmp}}}{\partial \mathbf{x}}(t) \\ &= -A(u(t))^\top \Pi(t) - (1 - \alpha) v(t) \mathbf{g}(u(t)) \\ &\quad - v(t) J(\mathbf{x}(t), u(t))^\top \Lambda(t), \end{aligned} \quad (23)$$

$$\begin{aligned} \dot{\Lambda}(t) &= -\frac{\partial H_{\text{pmp}}}{\partial \mathbf{y}}(t) \\ &= -A(u(t))^\top \Lambda(t) - \alpha \beta v(t) \mathbf{g}(u(t)), \end{aligned} \quad (24)$$

$$\begin{aligned} \dot{p}(t) &= -\frac{\partial H_{\text{pmp}}}{\partial u}(t) \\ &= -\Lambda(t)^\top \partial_u A(u(t)) \mathbf{y}(t) - \Pi(t)^\top \partial_u A(u(t)) \mathbf{x}(t) \\ &\quad - v(t) [(1 - \alpha) \partial_u \mathbf{g}(u(t))^\top \mathbf{x}(t) + \alpha \beta \partial_u \mathbf{g}(u(t))^\top \mathbf{y}(t)] \\ &\quad - v(t) \Lambda(t)^\top \partial_u \mathbf{s}(\mathbf{x}(t), u(t)). \end{aligned} \quad (25)$$

For effective calculation, $\partial_u A(u(t))$ should be computed analytically in advance.

Finally in step 4, $\mathbf{g}(u)$ denotes the vectorized form of the operator $G(u)$, satisfying $\text{tr}[G(u)\rho] = \mathbf{g}(u)^\top \mathbf{x}$, and the Jacobian is defined as $J(\mathbf{x}, u) := \partial \mathbf{s}(\mathbf{x}, u) / \partial \mathbf{x}$. Then, the gradient with respect to the control $v(t)$ can be calculated as

$$\begin{aligned}\delta v(t) &:= \frac{\partial H_{\text{pmp}}}{\partial v}(t) \\ &= (1 - \alpha) \mathbf{g}(u(t))^\top \mathbf{x}(t) + \alpha \beta \mathbf{g}(u(t))^\top \mathbf{y}(t) \\ &\quad + p(t) + \mathbf{\Lambda}(t)^\top \mathbf{s}(\mathbf{x}(t), u(t)).\end{aligned}\quad (26)$$

III. NUMERICAL EXAMPLE

A. Two level spin-boson model

As a numerical example, we consider the following single spin system in a bosonic reservoir [18, 26]. The dynamics is described by the Lindblad equation

$$\begin{aligned}\dot{\rho}(t) &= \mathcal{L}_t(\rho(t)) \\ &= -i[H(t), \rho(t)] \\ &\quad + \gamma_\downarrow(E(t)) \left(\sigma_-(t)\rho(t)\sigma_+(t) - \frac{1}{2}\{\sigma_+(t)\sigma_-(t), \rho(t)\} \right) \\ &\quad + \gamma_\uparrow(E(t)) \left(\sigma_+(t)\rho(t)\sigma_-(t) - \frac{1}{2}\{\sigma_-(t)\sigma_+(t), \rho(t)\} \right),\end{aligned}\quad (27)$$

where $H(t) = u(t)\sigma_z + \Delta\sigma_x$. We work in a fixed basis $\{|g\rangle, |e\rangle\}$ and define $\sigma_z := |e\rangle\langle e| - |g\rangle\langle g|$, $\sigma_x := |e\rangle\langle g| + |g\rangle\langle e|$. Let $|e(t)\rangle$ and $|g(t)\rangle$ denote the instantaneous excited and ground eigenstates of $H(t)$, forming an orthonormal basis, and define the corresponding jump operators $\sigma_+(t) := |e(t)\rangle\langle g(t)|$ and $\sigma_-(t) := |g(t)\rangle\langle e(t)|$. For the spin-boson model, the transition rates are given by

$$\begin{aligned}\gamma_\downarrow(E) &= \gamma(E)(P(E) + 1), \\ \gamma_\uparrow(E) &= \gamma(E)P(E),\end{aligned}\quad (28)$$

where $\gamma(E) = kE^3$ (we set $k = 1$) and $P(E) = (e^{2\beta E} - 1)^{-1}$ is the Bose-Einstein distribution, where $E(t) := \sqrt{u(t)^2 + \Delta^2}$ is the energy gap and the rotation angle is defined by

$$\cos \theta = \frac{u}{E}, \quad \sin \theta = \frac{\Delta}{E}.\quad (29)$$

Our aim is to optimize the protocol $u(t)$ in order to minimize dissipation and fluctuation between $u(0) = 0$ and $u(T) = 1$ at $\beta = 1$.

For this physical system, we select vectorization as $\mathbf{x} = [\rho_{gg}, \rho_{ee}, \Re \rho_{eg}, \Im \rho_{eg}]^\top$ and $\mathbf{y} = [Y_{gg}, Y_{ee}, \Re Y_{eg}, \Im Y_{eg}]^\top$. In this basis, the Lindblad generator takes the matrix form and can be written as $\dot{\mathbf{x}} = A(u(t))\mathbf{x}$, where

$$A(u(t)) = C(u(t)) + R(-\theta(t))L(E(t))R(\theta(t)).\quad (30)$$

Here $C(u)$ is the contribution of the commutator term $-i[H(t), \rho(t)]$, given by

$$C(u) = \begin{pmatrix} 0 & 0 & 0 & 2\Delta \\ 0 & 0 & 0 & -2\Delta \\ 0 & 0 & 0 & 2u \\ -\Delta & \Delta & -2u & 0 \end{pmatrix}.\quad (31)$$

The matrix $L(E)$ denotes the generator of the jump (dissipative) part in the instantaneous energy eigenbasis, and takes the form

$$L(E) = \begin{pmatrix} -\gamma_\uparrow(E) & \gamma_\downarrow(E) & 0 & 0 \\ \gamma_\uparrow(E) & -\gamma_\downarrow(E) & 0 & 0 \\ 0 & 0 & -\frac{\gamma_\Sigma(E)}{2} & 0 \\ 0 & 0 & 0 & -\frac{\gamma_\Sigma(E)}{2} \end{pmatrix},$$

$$\gamma_\Sigma(E) := \gamma_\uparrow(E) + \gamma_\downarrow(E).\quad (32)$$

The matrix $R(\theta)$ represents the basis rotation $\tilde{\rho} = \exp(-i\sigma_y\theta/2)\rho\exp(i\sigma_y\theta/2)$ in the above real vectorization x , and is given by

$$R(\theta) = \begin{pmatrix} \frac{1 + \cos \theta}{2} & \frac{1 - \cos \theta}{2} & \sin \theta & 0 \\ \frac{1 - \cos \theta}{2} & \frac{1 + \cos \theta}{2} & -\sin \theta & 0 \\ -\frac{\sin \theta}{2} & \frac{\sin \theta}{2} & \cos \theta & 0 \\ 0 & 0 & 0 & 1 \end{pmatrix},\quad (33)$$

$$R(-\theta) = R(\theta)|_{\sin \theta \mapsto -\sin \theta}.\quad (34)$$

In this basis, the vectorized control operator $\mathbf{g}(u)$, defined by $\text{tr}[G(u)\rho] = \mathbf{g}(u)^\top \mathbf{x}$, is constant and given by $\mathbf{g} = [-1, 1, 0, 0]^\top$ which corresponds to $G(u) = \sigma_z$. In this setting, since $\dot{H}(t) = v(t)\sigma_z$, the anticommutator term in Eq. (6) satisfies

$$S_\rho(\dot{H}(t)) = v(t)S_\rho(\sigma_z), \quad S_\rho(\sigma_z) := \frac{1}{2}\{\rho, \Delta_\rho \sigma_z\}_+.\quad (35)$$

Since ρ is a density operator, we use $\rho_{gg} + \rho_{ee} = 1$ to simplify the explicit expression of $S_\rho(\sigma_z)$. Upon vectorization, $\text{vec}(S_\rho(\sigma_z)) = \mathbf{s}(\mathbf{x})$ takes the form

$$\mathbf{s}(\mathbf{x}) = \begin{pmatrix} -2x_1x_2 \\ 2x_1x_2 \\ (x_1 - x_2)x_3 \\ (x_1 - x_2)x_4 \end{pmatrix},\quad (36)$$

where we used the state vector components $x_1 = \rho_{gg}$, $x_2 = \rho_{ee}$, $x_3 = \Re \rho_{eg}$, and $x_4 = \Im \rho_{eg}$. Consequently, the Jacobian $J(\mathbf{x}) = \partial \mathbf{s} / \partial \mathbf{x}$ is given by

$$J(\mathbf{x}) = \begin{pmatrix} -2x_2 & -2x_1 & 0 & 0 \\ 2x_2 & 2x_1 & 0 & 0 \\ x_3 & -x_3 & x_1 - x_2 & 0 \\ x_4 & -x_4 & 0 & x_1 - x_2 \end{pmatrix}.\quad (37)$$

We precompute $\partial_u A(u(t))$ analytically to evaluate Eq. (25), as detailed in Appendix C. We also evaluate

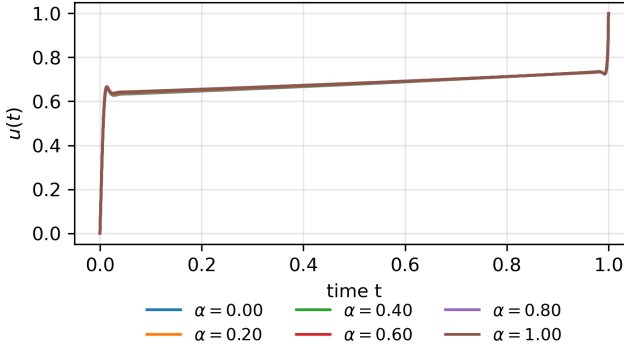


FIG. 1. Optimized control field $u(t)$ obtained by the GRAPE algorithm when $\Delta = 0$ for several values of the weight parameter α in the cost functional, as indicated in the legend, for protocol duration $T = 1$

Eq. (21) numerically with $E_T = \sqrt{u(T)^2 + \Delta^2}$, which yields

$$p(T) = (1 - \alpha) \tanh(\beta E_T) \frac{u(T)}{E_T} + \kappa(u(T) - u_T). \quad (38)$$

Using the component-wise representations introduced above, we implement the numerical procedure described in the Methods section.

The numerical settings used in the calculations are as follows. We discretize the time interval $[0, T]$ into N uniform steps with $\Delta t = T/N$. In practice, we choose N so that the time step is kept fixed across different protocol durations; specifically, we use $N = 1,000$ for $T = 1$ and $N = 10,000$ for $T = 10$. The control is parameterized by $v(t) = \dot{u}(t)$ and represented as a piecewise-constant function on each interval $[t_k, t_{k+1})$, while $u(t)$ is obtained by forward integration, $u_{k+1} = u_k + \Delta t v_k$, with the fixed initial condition $u(0) = u_0$. We use an explicit Euler scheme for the forward propagation of $x(t)$ and $y(t)$ and for the backward propagation of the adjoint variables. We initialize the optimization with a linear ramp connecting u_0 and u_T (i.e., constant $v = (u_T - u_0)/T$), and update v by gradient descent with learning rate η for up to $N_{\text{iter}} = 10^6$ iterations. We take $\eta = 0.01$ for $T = 1$ and $\eta = 0.001$ for $T = 10$. The terminal condition is enforced via the quadratic penalty $\frac{\kappa}{2}(u(T) - u_T)^2$ with $\kappa = 10.0$. For numerical stability, we allow box bounds $u(t) \in [-8, 8]$ and $v(t) \in [-100, 100]$ (implemented via projection after each update); for all results reported here these bounds are inactive, i.e., $u(t)$ and $v(t)$ remain well within the prescribed ranges. Unless otherwise stated, we set $\beta = 1$.

For the short-duration case ($T = 1$) with $\Delta = 0$ (i.e., $H(t) = u(t)\sigma_z$), Fig. 1 shows that the optimal protocol develops sharp jumps at both endpoints without imposing such a structure *a priori*, starting from a linear initial guess. Moreover, as discussed in Ref. [17] and Sec. A, the rapid-driving limit is known to yield protocols with endpoint jumps and an approximately constant value in

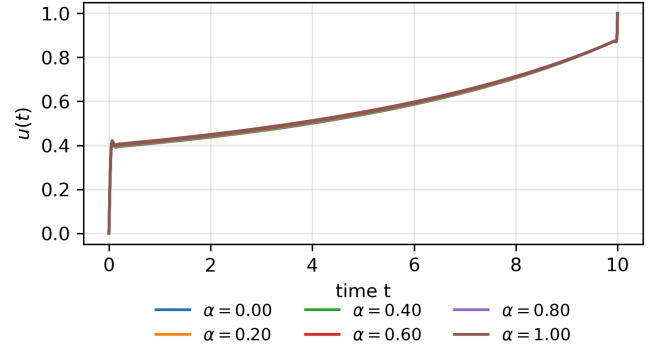


FIG. 2. Optimized control field $u(t)$ obtained by the GRAPE algorithm when $\Delta = 0$ for several values of the weight parameter α in the cost functional, as indicated in the legend, for protocol duration $T = 10$

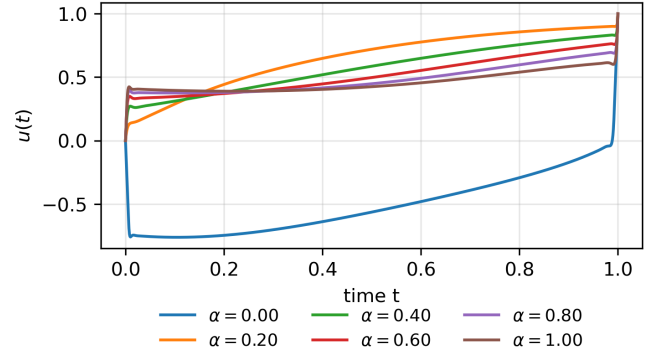


FIG. 3. Optimized control field $u(t)$ obtained by the GRAPE algorithm when $\Delta = 1$ for several values of the weight parameter α in the cost functional, as indicated in the legend, for protocol duration $T = 1$

between. In this case, the protocol depends only weakly on α , suggesting that dissipation and fluctuations can be optimized simultaneously.

As shown in Fig. 2, for the longer protocol duration $T = 10$, the optimal protocol still exhibits jumps at the beginning and the end; however, the intermediate segment is no longer approximately constant, indicating a departure from the rapid-driving approximation.

For another example $\Delta = 1$, $H(t) = u(t)\sigma_z + \sigma_x$, as shown in Fig. 3, the optimal protocol minimizing dissipation and fluctuations differs. The Pareto front shown in Fig. 4 shows that the trade-off between the objectives differs qualitatively, and part of the Pareto front is missing.

As another example, for $\Delta = 1$ (i.e., $H(t) = u(t)\sigma_z + \sigma_x$), Fig. 3 shows that the optimal protocol depends strongly on the weight parameter α and differs qualitatively from the $\Delta = 0$ case. In particular, the dissipation-minimizing protocol (small α) and the fluctuation-minimizing protocol (large α) exhibit markedly different temporal structures rather than be-

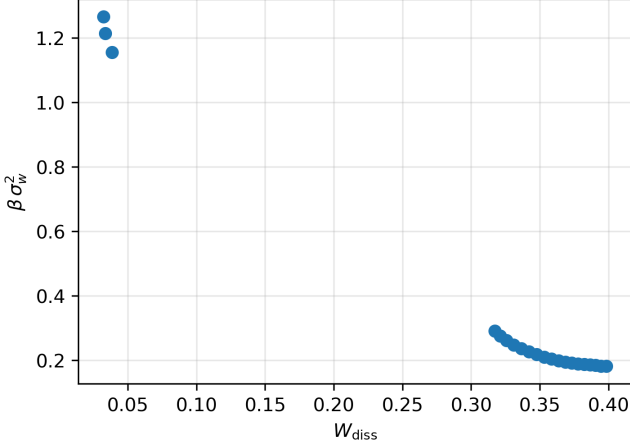


FIG. 4. Pareto front for the spin-boson model at $T = 1$, $\Delta = 1$ in the $(W_{\text{diss}}, \beta\sigma_w^2)$ plane. Each marker corresponds to an optimized protocol (obtained by GRAPE initialized from a linear ramp) for a given α , where α ranges from 0 to 1 in steps of 0.05.

ing related by a small deformation. The Pareto front in Fig. 4 indicates a qualitatively different trade-off between dissipation and fluctuations, and we observe a missing segment in the Pareto front. A plausible explanation is that the optimization switches between two distinct local minima corresponding to different protocol families as α is varied, which can leave an apparent gap when the intermediate trade-off solutions are not selected.

B. Quantum-dot model

As a second numerical example we consider a single-level quantum dot weakly coupled to a fermionic reservoir. We describe the empty and singly occupied dot states by the pseudo-spin basis $\{|g\rangle, |e\rangle\}$, with $\sigma_z|g\rangle = -|g\rangle$ and $\sigma_z|e\rangle = +|e\rangle$ as shown in the Appendix. E. The system Hamiltonian is again taken as

$$H(t) = u(t)\sigma_z, \quad (39)$$

where $u(t)$ now denotes half the level energy measured from the chemical potential of the lead, so that the single-particle excitation energy is $\varepsilon(t) = 2u(t)$. In contrast to the spin-boson model, $u(t)$ is allowed to take both positive and negative values, corresponding to moving the dot level above and below the Fermi energy.

In the weak-coupling and Markovian limit, and for a wide-band metallic lead at inverse temperature β with chemical potential set to zero, the dot dynamics is described by a fermionic Lindblad equation [24]. Since the control Hamiltonian is the same as in the $\Delta = 0$ spin-boson case, $H(t) = u(t)\sigma_z$, the corresponding control operator $G = \partial_u H = \sigma_z$ is unchanged. Therefore the auxiliary vector field $\mathbf{s}(\mathbf{x})$ and its Jacobian $J(\mathbf{x})$ are identical to Eqs. (36) and (37). The modification in the

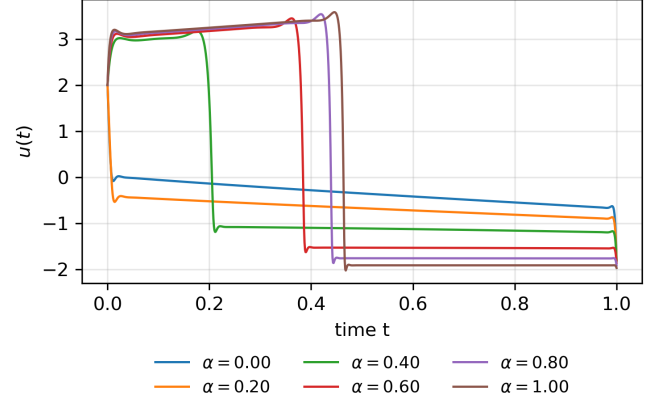


FIG. 5. FIG. 5. Optimized control field $u(t)$ obtained by the GRAPE algorithm for the quantum-dot model at $\beta = 1$ for several values of the weight parameter α in the cost functional, as indicated in the legend, for protocol duration $T=1$.

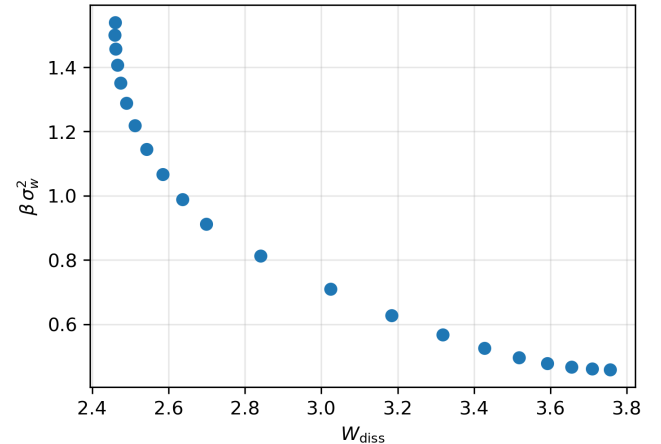


FIG. 6. Pareto front for the quantum-dot model at $\beta = 1$ in the $(W_{\text{diss}}, \beta\sigma_w^2)$ plane. Each marker corresponds to an optimized protocol (obtained by GRAPE initialized from a linear ramp) for a given α , where α ranges from 0 to 1 in steps of 0.05.

quantum-dot model enters through the dissipative transition rates, which are determined by the Fermi-Dirac distribution $f(u) = (1 + e^{2\beta u})^{-1}$ and a constant tunneling rate Γ :

$$\begin{aligned} \gamma_{\uparrow}(u) &= \Gamma f(u), \\ \gamma_{\downarrow}(u) &= \Gamma[1 - f(u)], \\ \gamma_{\Sigma}(u) &:= \gamma_{\uparrow}(u) + \gamma_{\downarrow}(u) = \Gamma, \end{aligned} \quad (40)$$

where we set $\Gamma = 1$. Accordingly, the vectorized generator $A(u)$ has the same matrix structure as in Eq. (30) (at $\Delta = 0$), with the rate-dependent entries given by $\gamma_{\uparrow,\downarrow}(u)$ above. Consequently, we can apply the same GRAPE optimization scheme as in the spin-boson case, imposing fixed boundary values $u(0) = u_0 = 2$ and $u(T) = u_T = -2$ and optimizing the protocol $v(t) = \dot{u}(t)$.

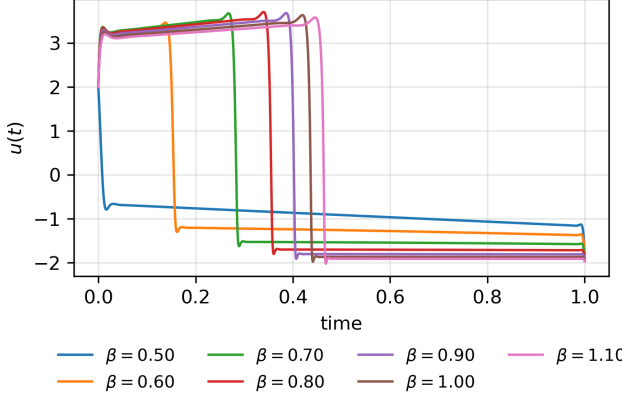


FIG. 7. Optimized control protocols $u(t)$ for the quantum-dot model obtained by GRAPE at $\alpha = 1$ for different inverse temperatures β , for protocol duration $T = 1$.

Firstly, we fix the inverse temperature at $\beta = 1$ and optimize the control protocol $v(t) = \dot{u}(t)$ for several values of the trade-off parameter α . The resulting optimal controls $u(t)$ are shown in Fig. 5. For small α , where the cost functional mainly penalizes dissipation, the protocols are shaped primarily to reduce W_{diss} and are consistent with the rapid-driving solution. As α is increased and more weight is placed on suppressing work fluctuations, the optimal solution changes qualitatively; beyond a certain range of α , $u(t)$ develops an additional intermediate jump and takes on a distinct protocol structure. Figure 6 shows the corresponding Pareto front at $\beta = 1$, i.e., the set of achievable pairs $(W_{\text{diss}}, \beta\sigma_w^2)$ obtained from the optimized protocols as α is varied.

Then, we fix $\alpha = 1$ (fluctuation minimization) and vary the inverse temperature β . Figure 7 shows the corresponding optimized protocols $u(t)$ for several values of β , obtained by GRAPE initialized from a linear ramp. For small β (high temperature), the protocols closely follow the rapid-drive solution consisting of two endpoint jumps separated by a single plateau. As β is increased, the numerically optimal protocol develops an additional intermediate jump and acquires a three-step structure. This trend is consistent with the fact that at high temperatures the Fermi-Dirac occupation $f(u) = (1 + e^{2\beta u})^{-1}$ depends only weakly on u , whereas at low temperatures $f(u)$ becomes increasingly step-like, so even modest changes in u drive the dot close to being fully occupied or empty and the rapid-drive approximation ceases to be valid.

IV. CONCLUSION

We have formulated a quantum optimal-control scheme which, for each value of the trade-off parameter α , minimizes a convex combination of dissipated work and work fluctuations for open quantum systems governed by time-

dependent Lindblad dynamics, up to an additional terminal penalty enforcing the boundary condition on $u(t)$. A key technical step is the introduction of an auxiliary operator $Y(t)$, which obeys linear time evolution and converts the originally double time integral of the TPM variance into a single-time integral. This allows W_{diss} and $\beta\sigma_w^2/2$ to be handled within a single time-local cost functional and yields explicit gradient expressions that can be used in GRAPE-like optimization algorithms based on Pontryagin's maximum principle.

We first apply this framework to a driven spin-boson model coupled to a bosonic reservoir, with controlled Hamiltonian $H(t) = u(t)\sigma_z + \Delta\sigma_x$ and a relaxation rate of the form $\gamma(E) \propto E^3$, which renders the slow-driving approximation unreliable near $E \simeq 0$. For the incoherent case ($\Delta = 0$), the optimized continuous protocols recover—for short protocol durations—the characteristic two-jump structure known from rapid-drive analysis, whereas for longer durations they exhibit clear deviations from those approximate solutions, thereby providing optimized protocols beyond the rapid-drive regime. For the coherent case ($\Delta \neq 0$), the optimal protocol depends strongly on the trade-off parameter α and the corresponding Pareto front indicates a qualitatively different dissipation–fluctuation trade-off, including an apparent missing segment consistent with switching between distinct locally optimal protocol families.

We then consider a quantum-dot model coupled to a wide-band metallic lead. In this setting, the optimization yields multi-step jump protocols with additional jumps in the interior of the protocol interval, which are not captured by the rapid-drive approximation. In the $(W_{\text{diss}}, \sigma_w^2)$ plane, these protocols produce a curved Pareto front, indicating a nontrivial trade-off between dissipation and work fluctuations: improving one of W_{diss} or σ_w^2 is accompanied by a comparatively large deterioration of the other.

Overall, our results suggest that time-continuous optimal control of Lindblad dynamics can be used to design driving protocols that balance dissipation and work fluctuations, at least in the examples considered here, in parameter regimes where the standard slow- or rapid-driving approximations are not sufficient. It would be interesting in future work to apply this optimization framework to systems with larger Hilbert spaces or additional control parameters, and to explore alternative cost functionals that incorporate further operational constraints.

Appendix A: rapid drive approximation

Under the rapid drive approximation [17], which assumes an initial and a final jump, with a constant segment between them, excess work and fluctuations in the

setting of section III A can be written as

$$W_{\text{diss}} = \beta^{-1} S(\pi(0) \parallel \pi(u_T)) + \int_0^T dt [u_T - u(t)] R(u(t)), \quad (\text{A1})$$

$$\sigma_w^2 = \beta^{-2} V(\pi(0) \parallel \pi(u_T)) \quad (\text{A2})$$

$$+ \int_0^T dt \{ [u_T - u(t)]^2 G(u(t)) \} \quad (\text{A3})$$

$$+ [u_T - u(t)] B(u(t)) u(t) \}, \quad (\text{A4})$$

Here S and V are relative entropy and relative entropy variance respectively.

$$S(\rho_1 \parallel \rho_2) = \text{Tr}[\rho_1 \log \rho_1] - \text{Tr}[\rho_1 \log \rho_2] \quad (\text{A5})$$

$$V(\rho_1 \parallel \rho_2) = \text{Tr}[\rho_1 (\log \rho_1 - \log \rho_2)^2] - S^2(\rho_1 \parallel \rho_2) \quad (\text{A6})$$

$R(u)$, $G(u)$ and $B(u)$ are defined as

$$R(u) := \text{Tr}[\sigma_z \mathcal{L}_u(\pi(0))], \quad (\text{A7})$$

$$G(u) := \frac{1}{2} \text{Tr}[\{\sigma_z, \sigma_z\}_+ \mathcal{L}_u(\pi(0))], \quad (\text{A8})$$

$$B(u) := \text{Tr}[\sigma_z \mathcal{L}_u(\{\sigma_z, \pi(0)\}_+)], \quad (\text{A9})$$

and $\pi(u) := e^{-\beta u \sigma_z} / (2 \cosh(\beta u))$, $\{\cdot, \cdot\}_+$ is the anticommutator, and $\gamma(u) = u^3$. The dissipation-minimizing jump ζ satisfies

$$\frac{d}{du} [(u_T - u) R(u)] \Big|_{u=\zeta} = 0, \quad (\text{A10})$$

while the fluctuation-minimizing jump Λ satisfies

$$\frac{d}{du} [(u_T - u)^2 G(u) + (u_T - u) B(u) u] \Big|_{u=\Lambda} = 0. \quad (\text{A11})$$

By applying these equations to our settings,

$$R(u) = -\gamma(u), \quad (\text{A12})$$

$$G(u) = 0, \quad (\text{A13})$$

$$B(u) = -2\gamma(u) \coth(\beta u), \quad (\text{A14})$$

with $\gamma(u) = u^3$. Then we obtain dissipation minimizing jump ζ and fluctuation minimizing jump Λ satisfy :

$$\zeta = \frac{3}{4} u_T, \quad (\text{A15})$$

$$(5\Lambda - 4u_T) \coth(\beta\Lambda) = \beta\Lambda(\Lambda - u_T) \operatorname{csch}^2(\beta\Lambda). \quad (\text{A16})$$

at $u_T = 1$, $\beta = 1$, optimal protocol jumps at $\zeta = 0.6$ and $\Lambda = 0.77$ respectively.

Appendix B: GRAPE algorithm

We use the GRAPE algorithm to optimize the protocol in this paper. We then summarize the algorithm from [22]. As a problem setting, the dynamics of the system is described as

$$\dot{q}(t) = f(q(t), u(t)), \quad (\text{B1})$$

where $q(t)$ is the state vector and $u(t)$ is the control parameter, and the cost function to be minimized during a fixed time duration $[0, T]$ is described as

$$J = \int_0^T f^0(q(t), u(t)) dt + d(T, q(T)). \quad (\text{B2})$$

Pontryagin Hamiltonian is defined as

$$\mathcal{H}(q, p, u) = p^\top f(q, u) + f^0(q, u), \quad (\text{B3})$$

where $p(t)$ is the costate variable. If $u(t)$ is optimal, then there exists an adjoint state $p(t)$ such that $(q(t), p(t), u(t))$ satisfies the necessary conditions of Pontryagin's principle:

$$\dot{q}(t) = \frac{\partial \mathcal{H}}{\partial p}(q(t), p(t), u(t)) = f(q(t), u(t)), \quad (\text{B4})$$

$$\dot{p}(t) = - \left(\frac{\partial \mathcal{H}}{\partial q}(q(t), p(t), u(t)) \right)^\top, \quad (\text{B5})$$

$$p(T) = - \left(\frac{\partial d(T, q)}{\partial q} \right)^\top \Big|_{q=q(T)}, \quad (\text{B6})$$

$$\frac{\partial \mathcal{H}}{\partial u}(q(t), p(t), u(t)) = 0. \quad (\text{B7})$$

In order to satisfy these equations, the GRAPE algorithm is as follows.

1. For a given trial control $u(t)$, propagate the state variable $q(t)$ forward in time by solving

$$\dot{q}(t) = f(q(t), u(t)), \quad q(0) = q_0. \quad (\text{B8})$$

2. Set the terminal value of the adjoint variable at $t = T$ as

$$p(T) = \left(\frac{\partial d(T, q)}{\partial q} \right)^\top \Big|_{q=q(T)}. \quad (\text{B9})$$

3. Propagate the adjoint variable $p(t)$ backward in time using the adjoint equation

$$\dot{p}(t) = - \left(\frac{\partial \mathcal{H}}{\partial q}(q(t), p(t), u(t)) \right)^\top. \quad (\text{B10})$$

4. Compute the gradient

$$g(t) = \frac{\partial \mathcal{H}}{\partial u}(q(t), p(t), u(t)),$$

and update the control according to

$$u(t) \rightarrow u(t) - \eta g(t),$$

with a suitable step size $\eta > 0$.

5. Repeat steps 1–4 until convergence of the cost.

Appendix C: calculation of $\partial_u A(u)$

We analytically calculate $\partial_u A(u)$ beforehand for the GRAPE algorithm.

$$\begin{aligned}\partial_u A(u) &= \partial_u C(u) + \partial_u \left(R(-\theta) L(E) R(\theta) \right) \\ &= \partial_u C(u) + (\partial_u R(-\theta)) L(E) R(\theta) \\ &\quad + R(-\theta) (\partial_u L(E)) R(\theta) + R(-\theta) L(E) (\partial_u R(\theta)).\end{aligned}\quad (\text{C1})$$

As defined in Eqs.(29),

$$\frac{dE}{du} = \frac{u}{E}, \quad \frac{d}{du} \cos \theta = \frac{\Delta^2}{E^3}, \quad \frac{d}{du} \sin \theta = -\frac{u\Delta}{E^3}.\quad (\text{C2})$$

The coherent contribution yields

$$\partial_u C(u) = \begin{pmatrix} 0 & 0 & 0 & 0 \\ 0 & 0 & 0 & 0 \\ 0 & 0 & 0 & 2 \\ 0 & 0 & -2 & 0 \end{pmatrix}.\quad (\text{C3})$$

Since $L(E)$ depends on u only through E , the chain rule gives

$$\begin{aligned}\partial_u L(E) &= \frac{dE}{du} \partial_E L(E) \\ &= \frac{u}{E} \begin{pmatrix} -\gamma'_\uparrow(E) & \gamma'_\downarrow(E) & 0 & 0 \\ \gamma'_\uparrow(E) & -\gamma'_\downarrow(E) & 0 & 0 \\ 0 & 0 & -\frac{\gamma'_\Sigma(E)}{2} & 0 \\ 0 & 0 & 0 & -\frac{\gamma'_\Sigma(E)}{2} \end{pmatrix}, \\ \gamma'_\Sigma(E) &= \gamma'_\uparrow(E) + \gamma'_\downarrow(E),\end{aligned}\quad (\text{C4})$$

where the prime denotes differentiation with respect to E . In particular, with Eqs. (28), we have

$$P'(E) = -2\beta P(E)(P(E) + 1),\quad (\text{C5})$$

$$\gamma'_\uparrow(E) = \gamma'(E)P(E) + \gamma(E)P'(E),\quad (\text{C6})$$

$$\gamma'_\downarrow(E) = \gamma'(E)(P(E) + 1) + \gamma(E)P'(E),\quad (\text{C7})$$

with $\gamma'(E) = 3E^2$.

Moreover, $R(\theta)$ depends on u through $c = \cos \theta$ and $s = \sin \theta$ in (34), so that

$$\partial_u R(\theta) = \frac{dc}{du} \partial_c R + \frac{ds}{du} \partial_s R,\quad (\text{C8})$$

with

$$\partial_c R = \begin{pmatrix} \frac{1}{2} & -\frac{1}{2} & 0 & 0 \\ -\frac{1}{2} & \frac{1}{2} & 0 & 0 \\ 0 & 0 & 1 & 0 \\ 0 & 0 & 0 & 0 \end{pmatrix}, \quad \partial_s R = \begin{pmatrix} 0 & 0 & 1 & 0 \\ 0 & 0 & -1 & 0 \\ -\frac{1}{2} & \frac{1}{2} & 0 & 0 \\ 0 & 0 & 0 & 0 \end{pmatrix}.\quad (\text{C9})$$

Since $R(-\theta)$ is obtained by the substitution $s \mapsto -s$, we have

$$\partial_u R(-\theta) = \frac{dc}{du} \partial_c R - \frac{ds}{du} \partial_s R.\quad (\text{C10})$$

Combining (C1) with (C2)–(C10) yields an explicit expression for $\partial_u A(u)$.

Appendix D: time evolution of $Y(t)$

In this section we derive the time evolution of the auxiliary operator defined in Eq. (9). By definition (7) and the Leibniz integral rule,

$$\partial_{t_1} \overleftarrow{\mathcal{P}}(t_1, t_2) = \mathcal{L}_{t_1} \overleftarrow{\mathcal{P}}(t_1, t_2), \quad \overleftarrow{\mathcal{P}}(t_2, t_2) = \mathcal{I}. \quad (\text{D1})$$

$$\begin{aligned}\frac{d}{dt} Y(t) &= \frac{d}{dt} \int_0^t \overleftarrow{\mathcal{P}}(t, \tau) [S_{\rho(\tau)}(\dot{H}(\tau))] d\tau \\ &= \overleftarrow{\mathcal{P}}(t, t) S_{\rho(t)}(\dot{H}(t)) + \int_0^t d\tau \frac{\partial}{\partial t} \overleftarrow{\mathcal{P}}(t, \tau) [S_{\rho(\tau)}(\dot{H}(\tau))] \\ &= S_{\rho(t)}(\dot{H}(t)) + \int_0^t d\tau \mathcal{L}_t \left[\overleftarrow{\mathcal{P}}(t, \tau) [S_{\rho(\tau)}(\dot{H}(\tau))] \right] \\ &= S_{\rho(t)}(\dot{H}(t)) + \mathcal{L}_t \left[\int_0^t d\tau \overleftarrow{\mathcal{P}}(t, \tau) [S_{\rho(\tau)}(\dot{H}(\tau))] \right] \\ &= S_{\rho(t)}(\dot{H}(t)) + \mathcal{L}_t [Y(t)]\end{aligned}$$

Then we obtain Eq. (10).

Appendix E: Equivalence between the Fock-space description of a single-level quantum dot and a two-level (pseudospin) representation

a. Quantum dot in the Fock basis. A single-level quantum dot (neglecting spin degeneracy) is naturally described in the fermionic Fock space spanned by the empty and occupied states $\{|0\rangle, |1\rangle\}$. The annihilation and creation operators a and a^\dagger act as

$$a|0\rangle = 0, \quad a|1\rangle = |0\rangle, \quad a^\dagger|0\rangle = |1\rangle, \quad a^\dagger|1\rangle = 0. \quad (\text{E1})$$

In the ordered basis $(|0\rangle, |1\rangle)$, these operators have the matrix representations

$$|0\rangle = \begin{pmatrix} 1 \\ 0 \end{pmatrix}, \quad |1\rangle = \begin{pmatrix} 0 \\ 1 \end{pmatrix}, \quad a = \begin{pmatrix} 0 & 1 \\ 0 & 0 \end{pmatrix}, \quad a^\dagger = \begin{pmatrix} 0 & 0 \\ 1 & 0 \end{pmatrix}. \quad (\text{E2})$$

Hence the number operator is

$$n = a^\dagger a = \begin{pmatrix} 0 & 0 \\ 0 & 1 \end{pmatrix} = |1\rangle\langle 1|. \quad (\text{E3})$$

The standard dot Hamiltonian is then

$$H_{\text{QD}}(t) = \varepsilon(t) a^\dagger a = \varepsilon(t) \begin{pmatrix} 0 & 0 \\ 0 & 1 \end{pmatrix}. \quad (\text{E4})$$

b. *Two-level-system representation.* For a generic two-level system, we use the basis $\{|g\rangle, |e\rangle\}$. In the ordered basis $(|g\rangle, |e\rangle)$, we represent the basis vectors as

$$|g\rangle = \begin{pmatrix} 1 \\ 0 \end{pmatrix}, \quad |e\rangle = \begin{pmatrix} 0 \\ 1 \end{pmatrix}. \quad (\text{E5})$$

The Pauli matrix σ_z is defined by

$$\sigma_z |g\rangle = -|g\rangle, \quad \sigma_z |e\rangle = +|e\rangle, \quad (\text{E6})$$

and therefore has the matrix representation

$$\sigma_z = \begin{pmatrix} -1 & 0 \\ 0 & 1 \end{pmatrix} \quad \text{in the basis } (|g\rangle, |e\rangle). \quad (\text{E7})$$

Identifying the Fock states with the two-level basis as

$$|g\rangle \equiv |0\rangle, \quad |e\rangle \equiv |1\rangle, \quad (\text{E8})$$

we may rewrite the projector $|1\rangle\langle 1|$ in terms of I and σ_z :

$$|1\rangle\langle 1| = \frac{I + \sigma_z}{2}. \quad (\text{E9})$$

Therefore,

$$H_{\text{QD}}(t) = \varepsilon(t) |1\rangle\langle 1| = \frac{\varepsilon(t)}{2} \sigma_z + \frac{\varepsilon(t)}{2} I. \quad (\text{E10})$$

The term proportional to I produces only an overall energy shift and can be dropped since it does not affect the density-matrix dynamics $([I, \rho] = 0)$. Defining the rescaled control amplitude

$$u(t) = \frac{\varepsilon(t)}{2}, \quad (\text{E11})$$

we obtain the effective two-level (pseudospin) Hamiltonian

$$H(t) = u(t) \sigma_z, \quad (\text{E12})$$

which is the form used in the main text. Thus, after a trivial rescaling of the Hamiltonian amplitude, the Fock-space description of the single-level quantum dot is equivalent to a two-level-system representation, and the same component-wise formalism can be applied.

ACKNOWLEDGMENTS

This work was supported by JSPS KAKENHI Grant Numbers JP23K24915 and JP24K03008.

[1] U. Seifert, “Stochastic thermodynamics, fluctuation theorems and molecular machines,” *Rep. Prog. Phys.* **75**, 126001 (2012).

[2] T. Schmiedl and U. Seifert, “Optimal finite-time processes in stochastic thermodynamics,” *Phys. Rev. Lett.* **98**, 108301 (2007).

[3] H. Then and A. Engel, “Computing the optimal protocol for finite-time processes in stochastic thermodynamics,” *Phys. Rev. E* **77**, 041105 (2008).

[4] S. Blaber, M. D. Louwense, and D. A. Sivak, “Steps minimize dissipation in rapidly driven stochastic systems,” *Phys. Rev. E* **104**, L022101 (2021).

[5] D. A. Sivak and G. E. Crooks, “Thermodynamic metrics and optimal paths,” *Phys. Rev. Lett.* **108**, 190602 (2012).

[6] A. P. Solon and J. M. Horowitz, “Phase transition in protocols minimizing work fluctuations,” *Phys. Rev. Lett.* **120**, 180605 (2018).

[7] F. Binder, L. A. Correa, C. Gogolin, J. Anders, and G. Adesso (eds.), *Thermodynamics in the Quantum Regime: Fundamental Aspects and New Directions*, Springer, Cham (2018).

[8] J. Kurchan, “A quantum fluctuation theorem,” [arXiv:cond-mat/0007360](https://arxiv.org/abs/cond-mat/0007360) (2000).

[9] H. Tasaki, “Jarzynski relations for quantum systems and some applications,” [arXiv:cond-mat/0009244](https://arxiv.org/abs/cond-mat/0009244) (2000).

[10] P. Talkner, E. Lutz, and P. Hänggi, “Fluctuation theorems: Work is not an observable,” *Phys. Rev. E* **75**, 050102(R) (2007).

[11] M. Campisi, P. Hänggi, and P. Talkner, “Colloquium: Quantum fluctuation relations: Foundations and applications,” *Rev. Mod. Phys.* **83**, 771 (2011).

[12] M. Esposito, U. Harbola, and S. Mukamel, “Nonequilibrium fluctuations, fluctuation theorems, and counting statistics in quantum systems,” *Rev. Mod. Phys.* **81**, 1665 (2009).

[13] S. Mukamel, “Quantum extension of the Jarzynski relation: Analogy with stochastic dephasing,” *Phys. Rev. Lett.* **90**, 170604 (2003).

[14] T. Monnai, “Unified treatment of the quantum fluctuation theorem and Jarzynski equality in terms of microscopic reversibility,” *Phys. Rev. E* **72**, 027102 (2005).

[15] S. Suomela, P. Solinas, J. P. Pekola, J. Ankerhold, and T. Ala-Nissila, “Moments of work in the two-point measurement protocol for a driven open quantum system,” *Phys. Rev. B* **90**, 094304 (2014).

[16] H. J. D. Miller, M. Scandi, J. Anders, and M. Perarnau-Llobet, “Work fluctuations in slow processes: Quantum signatures and optimal control,” *Phys. Rev. Lett.* **123**, 230603 (2019).

[17] A. Rolandi, M. Perarnau-Llobet, and H. J. D. Miller, “Optimal control of dissipation and work fluctuations for rapidly driven systems,” *New J. Phys.* **25**, 073005 (2023).

[18] H.-P. Breuer and F. Petruccione, *The Theory of Open Quantum Systems*, Oxford University Press, Oxford (2002).

[19] A. Rivas and S. F. Huelga, *Open Quantum Systems: An Introduction*, Springer, Berlin (2012).

[20] M. Scandi and M. Perarnau-Llobet, “Thermodynamic length in open quantum systems,” *Quantum* **3**, 197 (2019).

- [21] V. Cavina, A. Mari, A. Carlini, and V. Giovannetti, “Optimal thermodynamic control in open quantum systems,” *Phys. Rev. A* **98**, 012139 (2018).
- [22] U. Boscain, M. Sigalotti, and D. Sugny, “Introduction to the Pontryagin maximum principle for quantum optimal control,” *PRX Quantum* **2**, 030203 (2021).
- [23] N. Khaneja, T. Reiss, C. Kehlet, T. Schulte-Herbrüggen, and S. J. Glaser, “Optimal control of coupled spin dynamics: Design of NMR pulse sequences by gradient ascent algorithms,” *J. Magn. Reson.* **172**, 296–305 (2005).
- [24] U. Harbola, M. Esposito, and S. Mukamel, “Quantum master equation for electron transport through quantum dots and single molecules,” *Phys. Rev. B* **74**, 235309 (2006).
- [25] A. E. Allahverdyan and T. M. Nieuwenhuizen, “Fluctuations of work from quantum subensembles: The case against quantum work-fluctuation theorems,” *Phys. Rev. E* **71**, 066102 (2005).
- [26] T. Albash, S. Boixo, D. A. Lidar, and P. Zanardi, “Quantum adiabatic Markovian master equations,” *New J. Phys.* **14**, 123016 (2012).